Spectral and thermal management of hexagonal resonant structures for flexible opto-electronic transducers

Article · September 2024

DOI: 10.1016/j.optlastec.2024.110977

CITATIONS
0

READS
52

5 authors, including:

M.H. Elshorbagy
Minia University
51 PUBLICATIONS **396** CITATIONS
SEE PROFILE

Francisco J Gonzalez
University of Central Florida
241 PUBLICATIONS **3,347** CITATIONS
SEE PROFILE

Javier Alda
Complutense University of Madrid
233 PUBLICATIONS **2,686** CITATIONS
SEE PROFILE

Alexander Cuadrado
King Juan Carlos University
71 PUBLICATIONS **555** CITATIONS
SEE PROFILE

Optics & Laser Technology 176 (2024) 110977

Contents lists available at ScienceDirect

Optics and Laser Technology

journal homepage: www.elsevier.com/locate/optlastec

Full length article

Spectral and thermal management of hexagonal resonant structures for flexible opto-electronic transducers

Mahmoud H. Elshorbagy [a,b], Luis G. Torres-Lechuga [c], Francisco J. González [d], Javier Alda [a,*], Alexander Cuadrado [e]

[a] Applied Optics Complutense Group, Optics Department, Faculty of Optics and Optometry, Universidad Complutense de Madrid, Arcos de Jalón, 118, 28037 Madrid, Spain
[b] Physics Department, Faculty of Science, Minia University, El Minia, 61519, Egypt
[c] Coordinación para la innovación y Aplicación de la Ciencia y la Tecnología, Universidad Autónoma de San Luis Potosí(CIACYT), Av. Sierra Leona, 550, San Luis Potosí, 78210, Mexico
[d] Instituto Tecnológico de San Luis Potosí, Av. Tecnológico, San Luis Potosí, 78437, Mexico
[e] Escuela de Ciencias Experimentales y Tecnología, Universidad Rey Juan Carlos, Tulipán s/n, Móstoles, 28933, Madrid, Spain

ARTICLE INFO

Keywords:
Nanophotonics
Opto-electronic transduction
Metasurfaces
Resonant optics
Computational electromagnetism

ABSTRACT

Efficient on-chip optoelectronic devices in sensing and energy harvesting rely on the combination of subwavelength designs and multiphysical effects. In this contribution, we experimentally analyze and computationally model the optical performance of a hexagonal two-dimensional cluster placed over a silicon substrate and separated by a dielectric layer. Its reflectance has a dip in the long wavelength infrared band. This resonance is due to the generation of localized surface plasmons at the hexagonal surface. Our experimental results validate the multiphysics computational model which can be used to improve its performance as thermal detectors on flexible substrates. In this case, the model combines computational electromagnetism and heat transfer analysis to obtain the temperature distribution in the device. From this analysis, we have designed a thermal transducer based on a metasurface. It consists of a stacked arrangement made of a periodic hexagonal metallic array, a semiconductor ultra-thin layer, a metallic mirror, and a flexible substrate made of polyimide. The structure presented in this work behaves as a spectral selective surface with a resonant wavelength determined by the size of the hexagonal elements and the configuration of the multilayer. Our results show that this device has a time constant in the order of a few milliseconds (2.3 ms). This fast response can be useful in a wide variety of applications such as high speed thermal sensing and energy harvesting.

1. Introduction

Optical antennas and resonant structures have been proposed and developed as an adaptation of well-proven designs from the RF and microwave spectral ranges to the optical spectrum [1–3]. There are several limitations to transfer these classical antenna designs to the optical regime [4,5]. From a fundamental point of view, we are limited by the capabilities of materials to sustain oscillating currents at visible frequencies, the attenuation of optical fields within a volume determined by the skin depth of the material, and the disturbances in the charge carriers caused by surface defects [6–8]. From a practical point of view, as far as the dimensions of optical antennas are scaled with the wavelength, expensive and complex nano-fabrication tools are needed to comply with the expected resolution. At the same time, the finished surface should be smooth enough to sustain the movement of free charge carriers without significant disturbances. After considering these constrains, the capability of subwavelength structures to interact with light and to control the field distribution at the nanoscale has boosted the research and development of optical antennas and resonant structures. Modifications of these devices have been used as optical detectors with unique polarization and resonant properties. At the same time, it should be noted that an antenna provides an electrical signal generated by the received electromagnetic radiation. Classically, the transduction mechanism is a rectifying process, which is still being investigated for its efficiently application to optical frequencies [9–13]. Therefore, we denote an optical antenna as the combination of a resonant structure, capable of generating electrical currents through its morphology and material characteristics, plus a transducer that converts the optical radiation into an electrical signal [2,14–16]. As resonant elements not producing an electric transduction, if we are

* Corresponding author.
E-mail address: javier.alda@ucm.es (J. Alda).

https://doi.org/10.1016/j.optlastec.2024.110977
Received 20 December 2023; Received in revised form 6 March 2024; Accepted 3 April 2024
Available online 16 April 2024

interested in spectral selectivity, the main advantage of analyzing the parameters of metasurfaces is that we can make an educated choice of materials and geometrical parameters to control the spectral characteristics of the optical response for different applications. For example, in energy harvesting, we will be interested in having a strong absorption over a wide spectral range, while in sensing application we will be look for a narrow spectral response with a dependence on the sensed parameter. All these nanostructures are the main building blocks for a new kind of optical design that we call resonant optics [2,17,18].

In this contribution, we focus on the capability of infrared antennas to interact with the optical band of the thermal emission of the human body, as a black-body radiator at 310 K. At this temperature, we have the maximum of emitted power centered around $\lambda = 9.36$ μm [19]. Therefore, a light harvester able to scavenge this thermal radiated power should center its spectral responsivity in the long wave infrared radiation band (LWIR). To help in this direction, several approaches have been done to include flexible materials [20,21], and resonant structures acting as perfect absorbers both in the visible and the infrared [22–24]. For an optoelectronic energy converter, the resonant structure should be connected to a non-dissipative transducer able to extract power from the device. This transduction could be done through optical rectification of currents [9], or by using a thermoelectric effect, as the Seebeck mechanism [25]. Some other advanced detection strategies use nanophotonic elements to manage light absorption in semiconductor photodetectors [26]. On the other hand, if the system is used as a detector to monitor a given parameter related with the radiated power, a bolometric dissipative transducer could be used to fabricate small footprint microbolometers [27,28]. In both the Seebeck and bolometric mechanisms, the currents generated by the resonance heat the transducer structure by Joule effect and provide the desired change in temperature triggering the previously mentioned physical mechanisms. Furthermore, if our device working in the LWIR band is used for sensing, the optical source could be a laser, which provides a larger irradiance and generates a stronger signal on the detector [29].

The mix of optical, thermal, and electrical physical mechanisms are the base of bolometers, thermoelectric transducers, and energy harvesting devices at the infrared [30–33]. Plasmonic effects in metasurfaces reduce the response time and increase the conversion efficiency of these devices [34,35]. Designs based on Fabry–Perot cavity show a response that is tuneable over broadband [36,37]. These designs take benefit from the manipulation of electromagnetic waves at the far field region. When involving a resonant structure, its near field has a characteristic fast decay in space, and a high local electromagnetic field enhancement [38,39]. If the resonant element is brought close to a mirror, the image source methods predict that confined light will bounce from the mirror and, if the conditions are favorable, it will heat both the structure and the mirror until reaching total absorption [40,41]. Here, we aim to do that using a resonant structure close to a thin metallic film spaced with good thermal conductor. The optical and thermal characteristics, and the physics behind the design, are explored in detail along this contribution. Then, the results already reported in the literature are expanded here for hexagonal metallic patches. An appropriate variation of these patches, when coupled to high thermal conductivity materials, allows the design of fast detectors in the infrared band, having a response time of a few ms.

After this introductory section, Section 2 describes the fabrication, characterization, and modeling of a cluster of hexagonal resonant elements. This section is divided in three subsection to better distinguish among the contents. In fact, Section 2.3 contains the details of the simulation made in the optical domain for the elements fabricated on a Si substrate coated with a SiO_2 layer. The comparison between the experimental results and the numerical calculation serves to validate this optical model and obtain important features of the resonant structure in terms of polarization and electric field confinement. Based on the previous hexagonal cluster design, Section 3 develops a new kind of device which is optimized to totally absorb the incident radiation within a narrow spectral range. The absorbed power is converted into heat and generates a temperature distribution along the multilayer arrangement. The structure is optimized to have the metallic elements heated and rising its temperature. As a consequence of the nanoscale dimensions, the increase in temperature is very fast, with response times in the order of very few ms. Finally, Section 4 summarizes the main findings of this contribution.

2. Fabrication, characterization, and modeling

A hexagonal geometry, as the one proposed in this paper, has several interesting advantages. First of all, hexagons tessellate the plane as one of the most compact configurations. Its shape is much closer to the circular shape than a square geometry, involving a wider tolerance with respect to the polarization state of the incoming light. It also offers the capability to generate a structure with several geometric parameters and distributions like clusters or periodic arrays. This of great interest for sensing and energy harvesting applications because it allows to tune its geometry and material choice for optimal response over the selected spectral band.

2.1. Fabrication process

Fig. 1 represents the steps of the fabrication process of a hexagonal clustered structure made of silver (Ag) on a silicon substrate coated with a 300 nm-thick silicon dioxide (SiO_2). The structures were fabricated using a standard electron-beam lithography process, followed by metal deposition and lift-off. Briefly, the fabrication consists in depositing a thin and uniform layer of electron-sensitive material – polymethymethacrylate resist, PMMA – on a silicon substrate coated with SiO_2. PMMA is a positive resist commonly used in e-beam lithography. It shows high resolution but low sensitivity, requiring a dose of approximately 100 μC/cm^2, that has to be adjusted to the writing field. The deposition of the resist is carried out by spin-coating. A general rule of thumbs is that the thickness of the resist should be approximately three times the thickness of the film to be lifted off. The designed hexagonal pattern is transferred to the resist through electron beam lithography. This causes the breaking of chemical bonds at the exposed pattern. Then, the sample is immersed in a developer (MIBK:IPA) that removes the exposed resist revealing the substrate. Afterwards, in the sputtering process, the target material, silver, is bombarded by ions generated by an electrical discharge, creating a spray of the material that deposits on the patterned substrate. In the last lift-off step, the metallic film that was deposited over the resist is removed using a solvent (acetone or sodium chloride methylene), leaving only metal over the regions exposed by the electron-beam.

2.2. Characterization

The morphological characterization of the fabricated devices is made using optical and scanning electron microscopes (see Fig. 2a,b). The design has a distribution of clustered hexagons in rectangular unit cells of size $\approx 14.5 \times 12.36$ μm^2, where the whole sample covers an area of 250 × 250 μm^2. The individual hexagonal element has a regular shape with side equal to $s_h = 1.91$ μm. The gap between elements is $g = 0.42$ μm in average. The thickness of the hexagonal elements is $t_h \sim 70$ nm, measured by surface profilometry. The SEM photographies (see Fig. 2b,c) also reveal a random particulate on top of the hexagonal patches. This is formed during the sputtering process. However, their size is very small compared with the wavelengths of the spectral band under investigation, so they do not affect the optical response of the structure, adding some residual scattering.

Optically, the samples have been tested under an FTIR spectrometer (Vertex 70/Hyperion - Bruker) to characterize the spectral reflectance in the infrared. The results of the these measurements are presented in the next section in comparison with the simulated results.

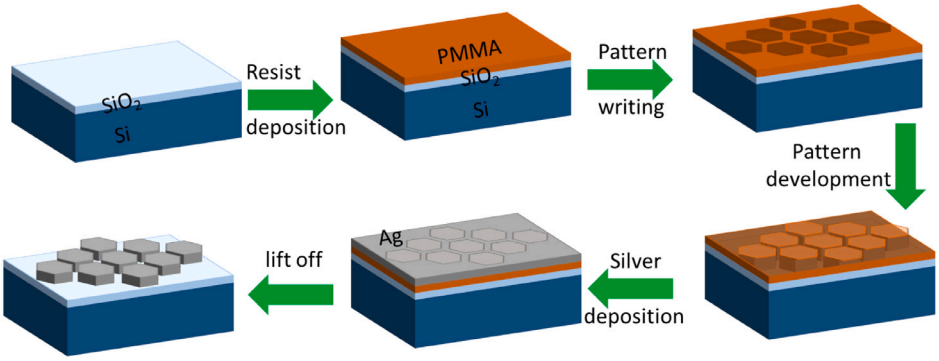

Fig. 1. The fabrication process start from top-left with a 500 μm thick silicon wafer substrate coated with 300 nm-thick SiO_2 layer. First a PMMA resist is spin coated on the Si/SiO_2 substrate, then a pattern is written on top of it using electron beam lithography. This pattern is revealed using a chemical that removes the un-exposed resists. Now, the sample is ready for metal deposition by sputtering, and finally, through a lift-off process, we obtain the designed structure. In our case, the deposited metal is Silver (Ag).

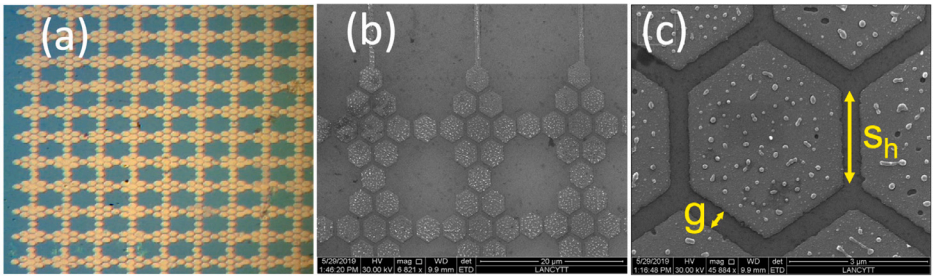

Fig. 2. (a) Optical microscopy photography of the spatial arrangement of the fabricated structure. View of the structure using a scanning electron microscope: (b) top view of the fabricated structure showing some clusters, (c) detail of the regular hexagons forming the clusters.

2.3. Optical model

For the computational electromagnetism model, the layered structure consists of a Si substrate coated with a SiO_2 layer of thickness, $t_{SiO_2} = 300$ nm. On top of it, we place a clustered hexagonal metallic structure with the same shape and dimensions as the fabricated sample (see Fig. 3a). To build the optical model, we used the Comsol Multiphysics software which is based on a finite element method. The dimensions of the hexagonal element, as the fabricated sample, have values of side length $s_h = 1.91$ μm, and a thickness $t_h = 70$ nm. The gap between each hexagon element within each cluster is set to $g = 0.3$ μm (see Fig. 3b). The unit cell in Fig. 3c shows the physical parameters of the optical model. The incident light is launched from a port placed on top of our structure, and separated enough to prevent any interference effects between the incident and reflected light. The settings of the excitation port define the incident wave as linearly polarized along the $x-$ or $y-$directions. The optical constants of the materials for each layer were extracted from recognized sources applicable to our design [42–44]. A receiving port is placed at the bottom of the structure to account for any transmitted light from the whole device. Floquet periodic boundary conditions are defined at each side of the unit cell to account for an infinite array. The whole geometry is meshed with a resolution that depends on the wavelength.

The optical losses depend on the square of the electric field amplitude and the complex optical constants of each layer according to the following equation [45]:

$$P(\omega) = \frac{1}{2}\omega\epsilon''(\omega)|E(\omega)|^2, \tag{1}$$

where $|E(w)|$ is the modulus of the electric field, ϵ'' is the imaginary part of the dielectric permittivity of the medium where the electric field propagates, and ω is the angular frequency of the electromagnetic radiation. $P(\omega)$ in Eq. (1) is evaluated locally and integrated within the volume of the element of interest. This evaluation is useful to compute how much energy dissipates in the structure and converts into heat.

In Fig. 4a, we have represented the modulus of the electric field for $\lambda = 8$ μm. The maps on the left and middle are for horizontal (oriented along the $x-$direction) and vertical (along the $y-$direction) linear polarizations, respectively. The map on the right corresponds with a cross section of the structure. These results show how the localized surface plasmon resonances (LSPR) enhance the electric field at the edges of the resonant patches aligned with the direction of polarization. At the same time, the responses of the hexagonal patches are coupled and interact among them. However, there is not a propagating wave along the structure, and the resonance remains localized [46,47]. The field distribution within the PML domains is null, which means that they efficiently absorb any field behind the ports. The functionality of the PML is of great importance to prevent interference effects between the ingoing and outgoing waves, which would give wrong values of the spectral parameters.

The field confinement in Fig. 4a right map represents a plasmonic absorption that appears as a dip in the spectral reflectance at $\lambda = 8$ μm. We can see this in Fig. 4b, where we checked the optical response of the structure for the horizontal and vertical polarizations represented in the left and middle maps of Fig. 4a. This evaluation confirm that both polarizations behave the same. The reason of this coincidence is the symmetry of the hexagonal shape, that is close to a rotationally symmetric geometry. The revealed polarization independent characteristic is of importance for energy harvesting application as the structure will be able to efficiently collect electromagnetic energy with any incident polarization (or even for the case of human body radiation, that is non polarized).

The model was validated by comparing the experimental and simulated spectral reflectances. As we can see in Fig. 4c, both lines agree well, except that the simulation spectral line is slightly wider compared with the experimental. Although not usual, this behavior has been also found in some other cases, and it could be caused by a mismatch in the index of refraction of the fabricated and simulated cases, or by slight variations in the values of the geometrical parameters [48].

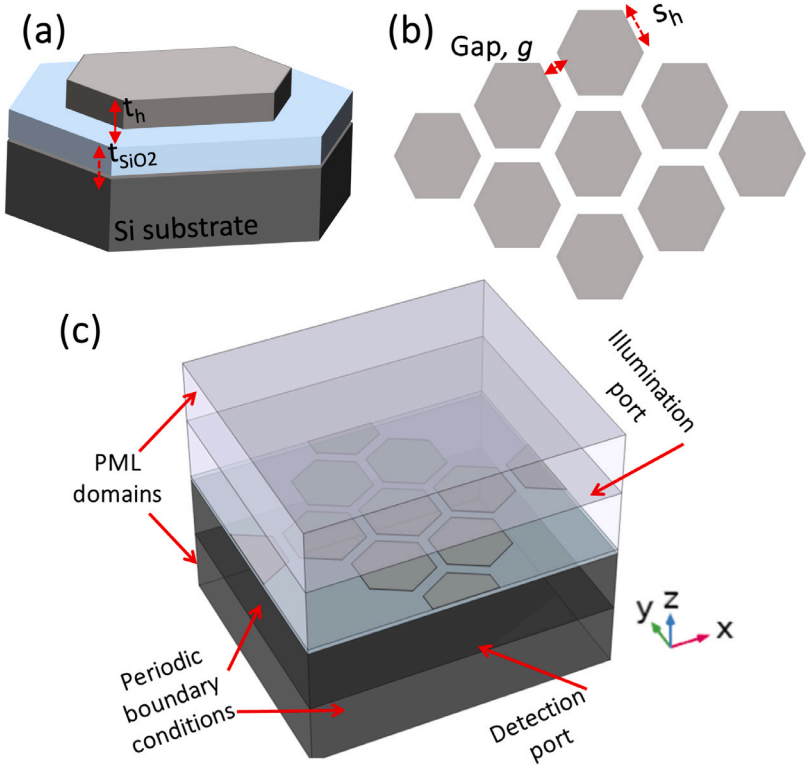

Fig. 3. (a) First model configuration of the hexagonal structures over SiO_2/Si substrate. (b) Hexagonal structures fabricated through electron beam lithography (EBL). (c) Geometric arrangement of the calculation cell for the hexagon cluster.

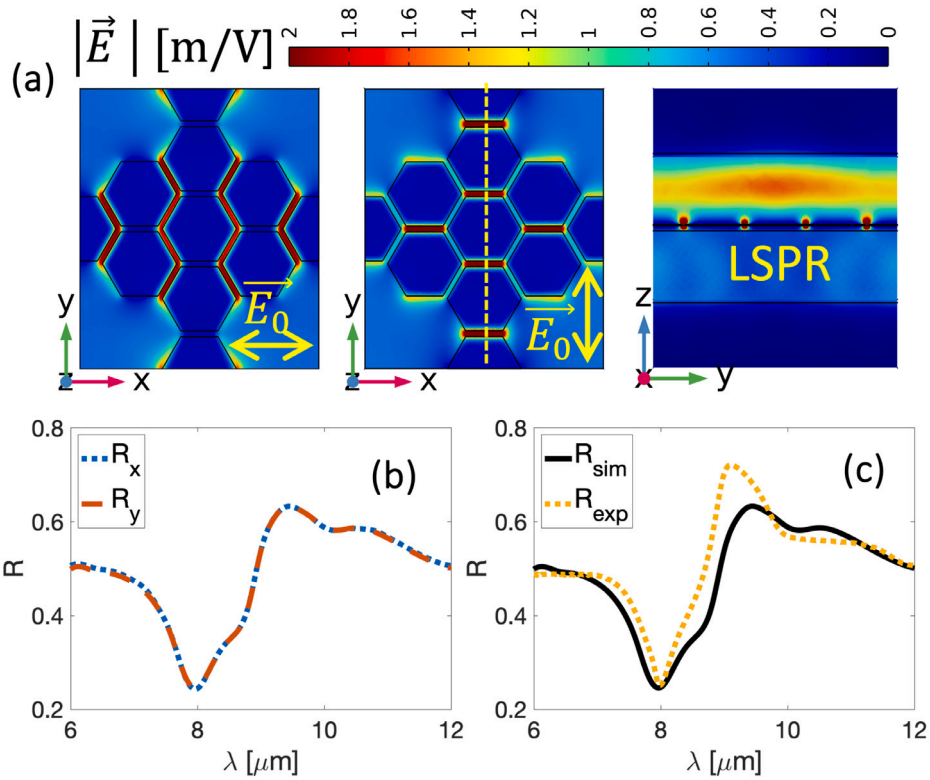

Fig. 4. (a) Modulus of the electric field for two linearly polarized illuminations: along the $x-$ direction in the left, and along y-direction in the map at the middle. The map to the right is a cross section along the yellow line drawn on the vertical polarization map. These maps have been obtained at $\lambda = 8$ μm. (b) Spectral reflectivity of the structure for the horizontal and vertical polarizations presented in (a). (c) Comparison between experiment (dotted line) and model (solid line) for the hexagonal cluster.

The spectral lineshape obtained here can find applications in sensing devices at the far infrared band. Furthermore, as the optical response is polarization insensitive, it will be useful in the design of thermal energy harvesting devices that benefit from both orthogonal components of the incoming electric field. As presented in this section, the optical model shows a good capability to reproduce the experimental response of the multilayer structure containing the clustered hexagonal metasurface. After this validation, we can use this model to develop new nanophotonic designs for energy harvesting and sensing applications.

3. Flexible optical absorber for thermal transduction

The next generation of energy harvesters and sensing devices needs flexible substrates and designs to fit with wearable mobile applications. A sound approach is to place efficient devices on top of flexible substrates without losing functionality and performance. The performance of these designs for different applications, especially sensing, depends on the involved physical mechanisms. If we are interested in gathering as much optical radiation as possible, perfect absorption based on plasmonic effect is a valuable strategy. From a practical point of view, it will be easy to extract the signal from a continuous metallic thin film layer instead of wiring metasurfaces with nano or micro connections over the gaps between individual elements. Besides being difficult to design, these interconnections may compromise the functionality of the whole device. However, metallic thin films are not good absorbers of electromagnetic waves. Instead, they reflect most of the incoming radiation, being very good mirrors. This is where nanophotonic mechanisms – including plasmonic resonances, scattering, and guiding effects – are at play to modify the reflectivity and to spatially redistribute the electromagnetic fields in a nanostructured multilayer system [23]. Our goal is to obtain a thin film structure having perfect absorption to directly convert electromagnetic radiation into heat [24]. To achieve this behavior, we build an hexagonal array above a continuous metallic film, spaced by a heat transport layer. In our case, the metallic metasurface will share the absorption with the metallic mirror below it, showing a strong dependence on the plasmonic resonance of the top structure. Helped by the heat transfer through the intermediate material, both metallic elements will raise their temperature, without significant loss in this transduction between optical and thermal mechanisms. This minimum heat loss can be achieved if the spacer is an ultra-thin layer (few tens of nanometers) and is made with a high thermal conductivity material as, for example, silicon. All this together, allows the use of thermoelectric or bolometric mechanisms to generate electric power, or an electric signal, respectively. The bolometric or thermoelectric circuit may use the continuous thin film as part of the transducer.

The designs depicted in Fig. 5a can be described from top to bottom as: a periodic resonant structure array/a heat transport layer/a thin metallic film/a flexible thermal insulator substrate. A practical realization of this design is presented in Fig. 5b. Hexagonal silver patches are on top of a Si thin layer that optically and thermally interfaces with a continuous thin-film made of silver deposited on a polyimide substrate. The selected substrate, is flexible, low cost, and also works as a thermal insulator with a thermal conductivity $\kappa_{\text{polyimide}} = 0.25$ W/(m K) [49]. Moreover, polyimide is flexible and can be easily applied on curved surfaces. Besides, it is bio-compatible allowing its use in bio-sensing. In this realization, the metallic mirror is made of silver. If the transduction mechanism is of bolometric nature, silver could be substituted by nickle because of its higher temperature coefficient of resistance [28]. If we use the thermoelectric effect, this metallic mirror would be made of two materials with opposite and high Seebeck coefficients, for example, Ni and Ti [25]. The high thermal conductivity material above the metallic mirror is Si, which is characterized by $\kappa_{\text{Si}} = 75$ W/(m K) at $T = 300$ K for a thickness of $t_{\text{Si}} = 160$ nm [50,51]. Finally, the resonant hexagonal patches are made of silver. This structure is shown in Fig. 5b.

The optical performance of our device is evaluated first at a wavelength $\lambda = 9.36$ μm, that corresponds to the maximum wavelength

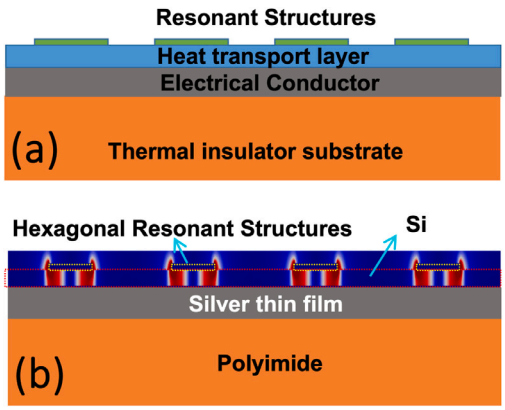

Fig. 5. (a) Schematic cross section of a device having spectrally selective total absorption. (b) Practical realization made on a polyimide substrate.

at which the human body, considered as a blackbody radiator, emit the most. Our model assumes assume a supersubstrate of air above the structure. The analysis begins with the calculation of the electric field distribution through the multilayer structure prior to the writing of the resonant hexagonal elements. Then this background field is used as input to a second study that calculates the absorption and scattering efficiency of the background field by the hexagonal structure. After an optimization process that maximizes absorption, we obtain the geometrical parameters of the structure. The hexagons dimensions are $s_h = 0.733$ μm, $g = 1.2$ μm, and $t_h = 70$ nm. The Si and metallic layers have thicknesses of $t_{\text{Si}} = 160$ nm, and $t_{\text{mirror}} = 200$ nm, respectively. Fig. 6a shows a map of the absorption in terms of the wavelength and the value of the side of the hexagonal structure. We can see that, as expected, a larger hexagon resonates at a larger wavelength following a linear dependence, $s_h = 0.1409\lambda - 0.4111$ μm, where λ should also be in microns [52]. Fig. 6b shows the plots of the spectral absorption and reflectance for the optimized structure. This plot reveals a maximum absorption at the desired wavelength. This absorption is shared by the metallic mirror at the bottom and the hexagonal structures on top.

When analyzing the electric field maps (see Fig. 5b), we saw how the hexagonal antenna resonates and alters the field distribution, redirecting it to the bottom. It was observed that the hexagonal antenna absorbs and concentrates the electric field according to the polarization state of the incoming electromagnetic radiation (see Fig. 4a). In our design, both the hexagons and the thin metal film will use this absorbed electromagnetic energy to generate heat. This heat dissipation generates a temperature increase ΔT when illuminated.

As far as our element increases the temperature of the device to trigger a thermoelectric mechanism or a bolometric effect, we have completed our analysis with a thermal simulation of the structure. The model contains two interlinked physical simulations: an electromagnetic evaluation using the optimized parameters, and a thermal simulation that uses the electromagnetic dissipated power as a heat source (see Eq. (1)). This thermal simulation includes the polyimide substrate to properly account for the heat transport through the full structure. Fig. 7a,b shows the variation in temperature at the metallic mirror for two cases of interest: a blackbody radiation at $T = 310$ K (human body temperature), and a laser source emitting at $\lambda = 9.36$ μm, that is the wavelength where the human body emits its maximum. The rise in temperature can be fitted to an exponential function of the form:

$$\delta T = \delta T_{\max}\left[1 - \exp\left(-\frac{t}{\tau}\right)\right], \tag{2}$$

where the fitting value of the time constant is $\tau = 2.3$ ms for both cases. This time response is considered fast compared with recent findings of recent reports [53–56], and can be of use when monitoring

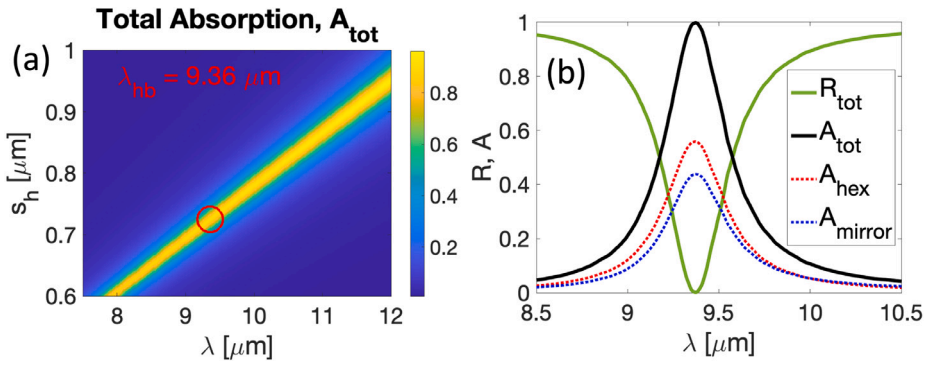

Fig. 6. (a) Map of the optical absorption in terms of the wavelength and side length of the hexagonal resonant structures. The red circle is located at the wavelength of interest, $\lambda = 9.36$ μm. (b) Absorption and Reflectance of the optimized structure. The contributions of the hexagonal elements (in black) and the metallic mirror (in blue) are represented with the total absorption (in green) and reflection (in red).

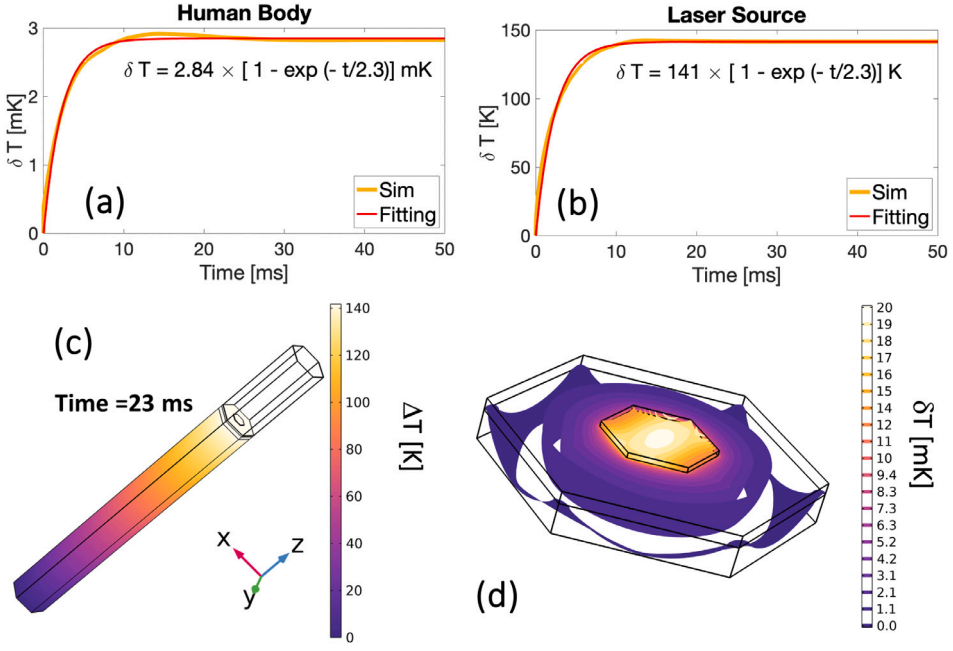

Fig. 7. Temperature vs. time graphs for: (a) the human body emission, and (b) a laser irradiation at $\lambda = 9.36$ μm. The equations inserted in these figures represent the application of Eq. (2) where t should be given in ms. In (c) we can see how the temperature decreases along the unit cell when moving from the resonant element towards the substrate. The temperature distribution around the resonant elements varies just 0.01% of the maximum raise in temperature. This temperature maps are calculated at $t = 23$ ms that is about 10 times the response time of the structure. The maps in figures (c) and (d) are different to show how the temperature changes very much along the whole structure and very little when close to the hexagonal patches.

rapid variations in optical radiation in the infrared, as it happens with combustion and explosive processes [57]. In Fig. 7 we show how the blackbody radiation representing the human body, with a irradiance of 19.96 W/m^2, can increase the temperature up to $\delta_{max} \simeq 2.83$ mK. At the same time, when using a laser source at $\lambda = 9.36$ μm having an irradiance of 100 W/cm^2, the temperature increases around $\delta T_{max} \simeq 142$ K. From the previous results we prove that polyimide is a good insulating substrate for this type of devices. The temperature distribution in the device is shown in Fig. 7c when $t = 23$ ms. When checking how the temperature distribution varies around the hexagons, we can see that the hexagonal patch is the hottest part, but only ≃0.01% above the temperature obtained at the mirror plane (see Fig. 7d), meaning that the Si thin layer is working efficiently as a good thermal conductor.

4. Conclusions

In this paper, we have presented an arrangement of hexagonal structures was designed with a distribution of clustered unit cells of size ≈14.5 × 12.36 μm^2, covering an area of 250 × 250 μm^2. The structure is fabricated on top of a Si substrate coated with 300 nm-thick SiO_2 layer. The manufactured hexagons have a side length, $s_h = 1.91$ μm. An optical model, based on the finite element method (Comsol Multiphysics), is built to reproduce the experimental spectral reflectance of the fabricated sample. We have checked that the optical response of this geometry is not dependent on the state of polarization of the incoming radiation. Moreover, the optical characterization of the fabricated structure show a good agreement with the model. The comparison between the simulation and the FTIR measurement of reflectance validated the computational electromagnetism approach used in this contribution.

Then, we have analyzed a metasurface made with a hexagonal array of resonant structures. When illuminated by infrared radiation, this design generates a temperature increase in the device through a total absorption process. This variation in temperature can be transduced to the electric domain through a bolometric or a thermoeledtric mechanism. The proposed idea may serve as a thermal energy scavenger when only thermal radiation is available, and also as a device producing a response proportional to the change in temperature generated by

infrared irradiance. The optimization of the geometrical parameters of our design was done using an optical and multiphysics (optical-thermal) model adapted to the proposed geometry. Our results included the evaluation of the electric field distribution, the spectral reflectance and absorption, and the distribution in temperature under the effect of electromagnetic radiation. The resonant structure efficiently channels a significant amount of energy downward. This phenomenon has been capitalized upon by incorporating a silicon layer, which aids in the heat transfer to a metallic layer. The metallic layer, in turn, receives and heats up through both conduction and the Joule effect.

We have assessed that the fabrication of infrared or optical antenna metasurfaces is an interesting study that would be worth exploring using different geometries and materials to increase absorption efficiency. In fact, the use of semiconductors and metals with adequate physical properties can enhance the desired response. For example, the selection of materials with a large difference in their Seebeck coefficients would increase the direct current produced for the case of a thermoelectric device.

CRediT authorship contribution statement

Mahmoud H. Elshorbagy: Writing – review & editing, Writing – original draft, Validation, Software, Methodology, Investigation, Formal analysis, Conceptualization. **Luis G. Torres-Lechuga:** Writing – review & editing, Writing – original draft, Visualization, Validation, Software, Methodology, Investigation, Formal analysis, Conceptualization. **Francisco J. González:** Writing – review & editing, Writing – original draft, Supervision, Methodology, Investigation, Formal analysis, Conceptualization. **Javier Alda:** Methodology, Investigation, Funding acquisition, Formal analysis, Conceptualization, Validation, Visualization, Writing – original draft, Writing – review & editing. **Alexander Cuadrado:** Writing – review & editing, Writing – original draft, Visualization, Validation, Software, Methodology, Funding acquisition, Formal analysis, Conceptualization.

Declaration of competing interest

The authors declare the following financial interests/personal relationships which may be considered as potential competing interests: Javier Alda reports financial support was provided by Ministerio de Economia y Competitividad. Alexander Cuadrado reports financial support was provided by Comunidad de Madrid. If there are other authors, they declare that they have no known competing financial interests or personal relationships that could have appeared to influence the work reported in this paper.

Data availability

Data will be made available on request.

Disclosures

The authors declare that AI has not being used for extracting or obtaining new information from the contents of the contribution.

Acknowledgments

This work has been partially supported by Ministerio de Economía *y* Competitividad through projects Nanorooms PID2019-105918GB-I00, and the program ‘‘Proyectos de I+D para jóvenes investigadores de la Universidad Rey Juan Carlos’’ through Comunidad de Madrid, under Grant 2022/00156/025 and Grant REF:M2742.

References

[1] J.H. Booske, R.J. Dobbs, C.D. Joye, C.L. Kory, G.R. Neil, G.-S. Park, J. Park, R.J. Temkin, Vacuum electronic high power terahertz sources, IEEE Trans. Terahertz Sci. Technol. 1 (1) (2011) 54–75.

[2] J. Alda, G. Boreman, Infrared Antenas and Resonant Structures, SPIE, 2017.

[3] J. Tian, T. Guo, N. He, J. Du, X. Hong, C. Fei, Z. Lin, R. Zhang, Q. Huang, Y. Wang, et al., Wide-field-of-view auto-coupling optical antenna system for high-speed bidirectional optical wireless communications in C band, Opt. Express 31 (20) (2023) 33435–33448.

[4] W. Geyi, Physical limitations of antenna, IEEE Trans. Antennas and Propagation 51 (8) (2003) 2116–2123.

[5] P. Bharadwaj, B. Deutsch, L. Novotny, Optical antennas, Adv. Opt. Photonics 1 (3) (2009) 438–483.

[6] J. Alda, J.M. Rico-Garcia, J.M. Lopez-Alonso, G. Boreman, Optical antennas for nano-photonic applications, Nanotechnology 16 (5) (2005) S230.

[7] F.J. González, J. Alda, Optical antennas as nano-probes in photonic crystals and dielectric waveguide structures, in: Proceedings of the Fourth European Conference on Antennas and Propagation, IEEE, 2010, pp. 1–3.

[8] K. Braun, F. Laible, O. Hauler, X. Wang, A. Pan, M. Fleischer, A.J. Meixner, Active optical antennas driven by inelastic electron tunneling, Nanophotonics 7 (9) (2018) 1503–1516, http://dx.doi.org/10.1515/nanoph-2018-0080.

[9] G. Moddel, S. Grover, Rectenna Solar Cells, Springer, 2013.

[10] C. Reynaud, D. Duché, J.-J. Simon, E. Sanchez-Adaime, O. Margeat, J. Ackermann, V. Jangid, C. Lebouin, D. Brunel, F. Dumur, et al., Rectifying antennas for energy harvesting from the microwaves to visible light: A review, Prog. Quantum Electron. 72 (2020) 100265.

[11] V. Balos, M. Wolf, S. Kovalev, M. Sajadi, Optical rectification and electro-optic sampling in quartz, Opt. Express 31 (8) (2023) 13317–13327.

[12] G.A. Khouqeer, N. Alanazi, A. Alodhayb, S. Chakraborty, V. Awasthi, S. Pandiaraj, G. Jayaswal, A study on bowtie antenna based optical rectenna system for THz energy harvesting applications, Opt. Quantum Electron. 55 (8) (2023) 674.

[13] R. Mupparapu, J. Cunha, F. Tantussi, A. Jacassi, L. Summerer, M. Patrini, A. Giugni, A. Alabastri, R.P. Zaccaria, Light rectification with plasmonic nano-cone point contact-insulator-metal architecture, in: Smart Materials for Opto-Electronic Applications, Vol. 12584, SPIE, 2023, pp. 105–114.

[14] A. Belkadi, A. Weerakkody, G. Lasser, G. Moddel, Demonstration of thermoradiative power generation using compensated infrared rectennas, ACS Photonics (2023).

[15] S. Tekin, S. Almalki, H. Finch, A. Vezzoli, L. O'Brien, V. Dhanak, S. Hall, I. Mitrovic, Electron affinity of metal oxide thin films of TiO_2, ZnO, and NiO and their applicability in 28.3 THz rectenna devices, J. Appl. Phys. 134 (8) (2023).

[16] H.-T. Nguyen, Z.-L. Yen, Y.-H. Su, Y.-P. Hsieh, M. Hofmann, 2D material-enabled optical rectennas with ultrastrong light-electron coupling, Small 18 (37) (2022) 2202199.

[17] V.E. Babicheva, Optical processes behind plasmonic applications, Nanomaterials 13 (7) (2023) 1270.

[18] S. Oldenburg, R. Averitt, S. Westcott, N. Halas, Nanoengineering of optical resonances, Chem. Phys. Lett. 288 (2–4) (1998) 243–247.

[19] J.D. Hardy, The radiation of heat from the human body, J. Clin. Invest. 13 (4) (1934) 593–604.

[20] A. Hazarika, B.K. Deka, C. Jeong, Y.-B. Park, H.W. Park, Biomechanical energy-harvesting wearable textile-based personal thermal management device containing epitaxially grown aligned Ag-tipped-$Ni_xco_{1-x}Se$ nanowires/reduced graphene oxide, Adv. Funct. Mater. 29 (31) (2019) 1903144.

[21] S. Zhang, J. Zhu, Y. Zhang, Z. Chen, C. Song, J. Li, N. Yi, D. Qiu, K. Guo, C. Zhang, et al., Standalone stretchable RF systems based on asymmetric 3D microstrip antennas with on-body wireless communication and energy harvesting, Nano Energy 96 (2022) 107069.

[22] S.K. Dubey, A. Kumar, G. Dayal, A. Pathak, S. Srivastava, Polarization insensitive metamaterial based electromagnetic multiband absorber in the long-wave infrared (LWIR) region, Opt. Laser Technol. 156 (2022) 108511, http://dx.doi.org/10.1016/j.optlastec.2022.108511, URL https://www.sciencedirect.com/science/article/pii/S0030399222006636.

[23] Z. Liu, H. Zhong, G. Liu, X. Liu, Y. Wang, J. Wang, Multi-resonant refractory prismoid for full-spectrum solar energy perfect absorbers, Opt. Express 28 (21) (2020) 31763–31774, http://dx.doi.org/10.1364/OE.405012, URL https://opg.optica.org/oe/abstract.cfm?URI=oe-28-21-31763.

[24] S. Li, W. Tan, X. Liu, G. Liu, Y. Wang, J. Chen, C. Tang, W. Du, Z. Liu, Efficient photothermal therapy with spatially localized high-temperature generation by refractory absorber, Appl. Phys. Lett. 123 (13) (2023) 131701, http://dx.doi.org/10.1063/5.0173805, arXiv:https://pubs.aip.org/aip/apl/article-pdf/doi/10.1063/5.0173805/18140147/131701_1_5.0173805.pdf.

[25] E. Briones, J. Briones, A. Cuadrado, J.C. Martinez-Anton, S. McMurtry, M. Hehn, F. Montaigne, J. Alda, F.J. Gonzalez, Seebeck nanoantennas for solar energy harvesting, Appl. Phys. Lett. 105 (9) (2014) 093108, http://dx.doi.org/10.1063/1.4895028, arXiv:https://pubs.aip.org/aip/apl/article-pdf/doi/10.1063/1.4895028/14315609/093108_1_online.pdf.

[26] Y. Zhu, Z. Liu, C. Niu, Y. Pang, D. Zhang, X. Liu, J. Zheng, Y. Zuo, H. Xue, B. Cheng, High-speed and high-power germanium photodetector based on a trapezoidal absorber, Opt. Lett. 47 (13) (2022) 3263–3266, http://dx.doi.org/10.1364/OL.461673, URL https://opg.optica.org/ol/abstract.cfm?URI=ol-47-13-3263.

[27] S.J.M. Rao, D.-S. Kim, S. Namgung, D. Lee, Antenna-based reduced IR absorbers for high-performance microbolometers, Opt. Lett. 47 (24) (2022) 6305–6308, http://dx.doi.org/10.1364/OL.474768, URL https://opg.optica.org/ol/abstract.cfm?URI=ol-47-24-6305.

[28] A. Cuadrado, J. Alda, F.J. González, Multiphysics simulation for the optimization of optical nanoantennas working as distributed bolometers in the infrared, J. Nanophotonics 7 (1) (2013) 073093, http://dx.doi.org/10.1117/1.JNP.7.073093.

[29] Z. Du, R. Zhou, S. Luo, D. Zhao, W. Long, Q. Ling, Z. Yu, D. Chen, Tunable multi-band absorbers based on graphene metasurfaces for infrared sensing and switching, Opt. Commun. 534 (2023) 129320.

[30] B. Padha, I. Yadav, S. Dutta, S. Arya, Recent developments in wearable NEMS/MEMS-based smart infrared sensors for healthcare applications, ACS Appl. Electron. Mater. (2023).

[31] R. Mondal, M.A.M. Hasan, J.M. Baik, Y. Yang, Advanced pyroelectric materials for energy harvesting and sensing applications, Mater. Today (2023).

[32] A. Varpula, A. Murros, K. Sovanto, A. Rantala, D. Gomes-Martins, K. Tappura, J. Tiira, M. Prunnila, Uncooled nano-thermoelectric bolometers for infrared imaging and sensing, in: Optical Components and Materials XX, Vol. 12417, SPIE, 2023, pp. 135–144.

[33] A. Varpula, K. Tappura, J. Tiira, K. Grigoras, O.-P. Kilpi, K. Sovanto, J. Ahopelto, M. Prunnila, Nano-thermoelectric infrared bolometers, APL Photonics 6 (3) (2021).

[34] Y. Luo, Z. Liang, D. Meng, J. Tao, J. Liang, C. Chen, J. Lai, Y. Qin, L. Jinguang, Y. Zhang, Ultra-broadband and high absorbance metamaterial absorber in long wavelength infrared based on hybridization of embedded cavity modes, Opt. Commun. 448 (2019) 1–9.

[35] J. Chen, J. Wang, X. Li, J. Chen, F. Yu, J. He, J. Wang, Z. Zhao, G. Li, X. Chen, et al., Recent progress in improving the performance of infrared photodetectors via optical field manipulations, Sensors 22 (2) (2022) 677.

[36] P. Zhang, X.-H. Deng, L. Tao, P. Li, M. Lu, F. Guo, Y. Song, J. Yuan, Broadband actively tunable metamaterial absorber based on vanadium dioxide and Fabry-Perot cavity, Opt. Mater. 138 (2023) 113716.

[37] Y. Chang, S. Xu, B. Dong, J. Wei, X. Le, Y. Ma, G. Zhou, C. Lee, Development of triboelectric-enabled tunable Fabry-Pérot photonic-crystal-slab filter towards wearable mid-infrared computational spectrometer, Nano Energy 89 (2021) 106446.

[38] J. Chen, Z. Ye, F. Yang, Y. Yin, Plasmonic nanostructures for photothermal conversion, Small Sci. 1 (2) (2021) 2000055.

[39] K.-T. Lin, H. Lin, B. Jia, Plasmonic nanostructures in photodetection, energy conversion and beyond, Nanophotonics 9 (10) (2020) 3135–3163.

[40] I.D. Mayergoyz, D.R. Fredkin, Z. Zhang, Electrostatic (plasmon) resonances in nanoparticles, Phys. Rev. B 72 (2005) 155412, http://dx.doi.org/10.1103/PhysRevB.72.155412, URL https://link.aps.org/doi/10.1103/PhysRevB.72.155412.

[41] H. Hu, Y. Xu, Z. Hu, B. Kang, Z. Zhang, J. Sun, Y. Li, H. Xu, Nanoparticle-on-mirror pairs: building blocks for remote spectroscopies, Nanophotonics 11 (22) (2022) 5153–5163, http://dx.doi.org/10.1515/nanoph-2022-0521.

[42] H.-J. Hagemann, W. Gudat, C. Kunz, Optical constants from the far infrared to the x-ray region: Mg, Al, Cu, Ag, Au, Bi, C, and Al_2O_3, J. Opt. Soc. Am. A 65 (6) (1975) 742–744.

[43] D. Chandler-Horowitz, P.M. Amirtharaj, High-accuracy, midinfrared (450 $cm^{-1} \leq \omega \leq$ 4000 cm^{-1}) refractive index values of silicon, J. Appl. Phys. 97 (12) (2005).

[44] J. Kischkat, S. Peters, B. Gruska, M. Semtsiv, M. Chashnikova, M. Klinkmüller, O. Fedosenko, S. Machulik, A. Aleksandrova, G. Monastyrskyi, et al., Mid-infrared optical properties of thin films of aluminum oxide, titanium dioxide, silicon dioxide, aluminum nitride, and silicon nitride, Appl. Opt. 51 (28) (2012) 6789–6798.

[45] J. Boroumand, S. Das, A. Vázquez-Guardado, D. Franklin, D. Chanda, Unified electromagnetic-electronic design of light trapping silicon solar cells, Sci. Rep. 6 (1) (2016) 31013.

[46] R.B. Schasfoort, Handbook of Surface Plasmon Resonance, second ed., Royal Society of Chemistry, 2017.

[47] M. Couture, S.S. Zhao, J.-F. Masson, Modern surface plasmon resonance for bioanalytics and biophysics, Phys. Chem. Chem. Phys. 15 (2013) 11190–11216, http://dx.doi.org/10.1039/C3CP50281C.

[48] R.C. Ng, J.C. Garcia, J.R. Greer, K.T. Fountaine, Polarization-independent, narrowband, near-IR spectral filters via guided mode resonances in ultrathin a-Si nanopillar arrays, ACS Photonics 6 (2) (2019) 265–271, http://dx.doi.org/10.1021/acsphotonics.8b01253, arXiv:https://doi.org/10.1021/acsphotonics.8b01253.

[49] B. Liu, Y. Zhou, L. Dong, Q. Lu, X. Xu, Enhanced thermal conductivity in copolymerized polyimide, Iscience 25 (11) (2022).

[50] C.J. Glassbrenner, G.A. Slack, Thermal conductivity of silicon and germanium from 3K to the melting point, Phys. Rev. 134 (1964) A1058–A1069, http://dx.doi.org/10.1103/PhysRev.134.A1058, URL https://link.aps.org/doi/10.1103/PhysRev.134.A1058.

[51] W. Liu, M. Asheghi, Thermal conductivity measurements of ultra-thin single crystal silicon layers, J. Heat Transfer 128 (1) (2005) 75–83, http://dx.doi.org/10.1115/1.2130403, arXiv:https://asmedigitalcollection.asme.org/heattransfer/article-pdf/128/1/75/5641338/75_1.pdf.

[52] Q.-H. Park, Optical antennas and plasmonics, Contemp. Phys. 50 (2) (2009) 407–423.

[53] B. Wu, Z. Zhang, B. Chen, Z. Zheng, C. You, C. Liu, X. Li, J. Wang, Y. Wang, E. Song, et al., One-step rolling fabrication of VO_2 tubular bolometers with polarization-sensitive and omnidirectional detection, Sci. Adv. 9 (42) (2023) eadi7805.

[54] X. Tu, P. Xiao, L. Kang, C. Jiang, X. Guo, Z. Jiang, R. Su, X. Jia, J. Chen, P. Wu, Nb_5n_6 microbolometer for sensitive, fast-response, 2-μm detection, Opt. Express 26 (12) (2018) 15585–15593.

[55] A. Abdullah, A. Koppula, O. Alkorjia, M. Almasri, Uncooled two-microbolometer stack for long wavelength infrared detection, Sci. Rep. 13 (1) (2023) 3470.

[56] M. Jiang, H. Xing, L. Zhang, L. Han, K. Zhang, C. Yao, D. Wang, X. Wang, S. Lan, X. Lv, et al., Fast switching of bolometric and self-powered effects in 2H-$NbSe_2$ for high-efficiency low-energy photon harvesting, Adv. Opt. Mater. 11 (12) (2023) 2300074.

[57] A.A. Chernov, K.V. Toropetsky, O.P. Korobeinichev, Estimation of the characteristic time scale of a laminar flame by particle image velocimetry, Combust. Explos. Shock Waves 59 (6) (2023) 686–692, http://dx.doi.org/10.1134/s0010508223060035.